Asitha C. Athukorala, Dennis V. De Pellegrin, Kyriakos I. Kourousis, Characterisation of head-hardened rail steel in terms of cyclic plasticity response and microstructure for improved material modelling Wear 2016, 366-367, pp. 416-424 (author accepted version)

Characterisation of head-hardened rail steel in terms of cyclic plasticity response and microstructure for improved material modelling

Asitha C. Athukorala [a], Dennis V. De Pellegrin[a], Kyriakos I. Kourousis[b,c]

[a] Queensland Universityof Technology, 2, GeorgeSt, Brisbane, QLD 4000, Australia

[b] Department of Mechanical, Aeronautical and Biomedical Engineering, University of Limerick, Co. Limerick, Limerick, Ireland

[c] School of Engineering, RMIT University, Melbourne, Victoria 3000, Australia

Abstract

Stress- and strain-controlled tests of heat treated high-strength rail steel (Australian Standard AS1085.1) have been performed in order to improve the characterization of the said material's ratcheting and fatigue wear behaviour. The hardness of the rail head material has also been studied and it has been found that hardness reduces considerably below four-millimetres from the rail top surface. Historically, researchers have used test coupons with circular cross-sections to conduct cyclic load tests. Such test coupons, typically five-millimetres in gauge diameter and ten-millimetres in grip diameter, are usually taken from the rail head sample. When there is considerable variation of material properties over the cross-section it becomes likely that localised properties of the rail material will be missed. In another case from the literature, disks 47 mm in diameter for a twin-disk rolling contact test machine were obtained directly from the rail sample and used to validate ratcheting and rolling contact fatigue wear models. The question arises: How accurate are such tests, especially when large material property gradients exist? In this research paper, the effects of rail sampling location on the ratcheting behaviour of AS1085.1 rail steel were investigated using rectangular-shaped specimens obtained at four different depths to observe their respective cyclic plasticity behaviour. The microstructural features of the test coupons were also analysed, especially the pearlite inter-lamellar spacing which showed strong correlation with both hardness and cyclic plasticity behaviour of the material. This work ultimately provides new data and testing methodology to aid the selection of valid parameters for material constitutive models to better understand rail surface ratcheting and wear.

Keywords— Rail steel; plasticity; ratcheting; wear; hardness; inter-lamellar spacing

1 Introduction

Railway systems play a crucial role in many countries in terms of social and economic development, especially countries like Australia, Canada, North America, South Africa and China which have mining-driven economies. In Australia, heavy-haul, intermodal and freight rail expertise is broad and diverse, operating the largest heavy-haul trains in the world (Fortescue Metals Group Ltd) with axle loads of 40-tonnes and a trailing load of 35.2 kilo-tonnes with 24 hours a day operation [1]. In comparison, the United

States of America, Canada and China have trailing loads of 22, 20.7 and 20 kilo-tonnes respectively, with axle loads under 30 tonnes. BHP Billiton in the Pilbara region of Western Australia runs iron-ore trains at 40-tonnes axle load on 68 kg/m rails, with maximum speeds of 75 km/h. In order to maintain such high levels of performance, the quality of rail materials is very important for reducing wear and other forms of rail degradation.

In Australia, heat treated high-strength hypereutectoid rail steel is used according to Australian Standards specification AS1085.1, exhibiting hardness in the range 360-420HV at the railhead. Standard rail steels have been supplied by different manufacturers potentially using different manufacturing processes and heat treatments to acquire the desired rail material properties. Material specifications aim to provide a benchmark for performance but it appears that field performance of the materials hasn't been studied comprehensively.

Rails are subjected to repetitive loads and the damage mechanism is governed by plastic deformation of the rail surface. This phenomenon is also known as cyclic plasticity. Rails are subjected to a variety of stress and strain conditions which can vary depending on location and severity of operation. Under stress-controlled cyclic behaviour, accumulation of plastic deformation called ratcheting takes place. The accumulated plastic strain is called the ratcheting strain.

Robust material modelling helps to make better predictions about the onset of rolling-contact fatigue and wear at the rail-wheel interface. The parameters used in material modelling may be obtained through stress- and strain-controlled cyclic load testing. Numerous researchers have carried out investigations on fatigue life and hardening/softening effects of materials under varying conditions of mean stress, amplitude and pre-load conditions.

In 2013, Pun et al. [2] performed an experimental study on the cyclic deformation characteristics and ratcheting behaviour of hypereutectoid high-strength rail steel used in Australian heavy-haul rail applications. They conducted tests on a 68 kg/m rail sample (50 and 60 kg/m rails are also commonly used in the industry [3]). Although Pun et al.'s study was limited to a low number of cycles (100-cycles typically), it was discovered that kinematic hardening is the dominant ratcheting behaviour of the material. The rail steel used in their research was premium rail steel which has relatively uniform material properties throughout the rail head.

Some researchers [4-8] have used material models to predict rail wear and the formation of other defects in the rail-wheel interface. The small twin-disk machines (SUROS and LEROS) used rail disks which were obtained from rail and wheel samples [7-10]. The results generated from the twin-disk machine tests using these wheels were subsequently used to validate the relevant wear models.

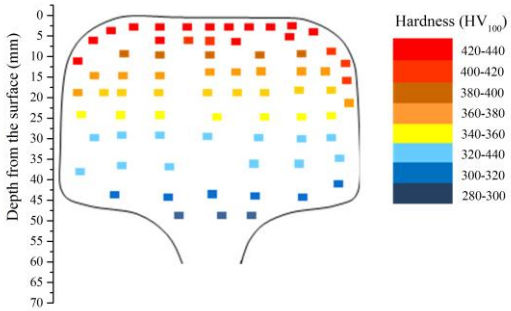

Fig. 1. Vickers hardness (HV100) data combined with the profile of the rail head.

From the present authors' work, hardness varies substantially across the cross-section of a heat-treated head-hardened rail, as shown in Fig. 1. According to the distribution profile, hardness reduces considerably as depth increases. Thus, it is apparent that errors would arise in the prediction of wear and ratcheting behaviour using test-wheels obtained from rails with significantly varying material properties.

Table 1. Chemical composition

Element	Composition
C	0.7% - 0.82%
Mn	0.7% - 1.1%
P	0.04%
S	0.04%
Si	0.1% - 0.35%

Problems may also arise with cyclic load tests used for material modelling where significant hardness gradients exist across the test coupons. This problem is less pronounced for quasi-homogeneous materials, where it should be sufficient to scale plastic properties in proportion to hardness [2]. Therefore, it is acceptable to use cylindrical test coupon to determine cyclic plasticity for the rail materials with small gradients in hardness and microstructure [11-13]. Surface hardened rail materials exhibit higher gradients of hardness and microstructure and therefore it becomes necessary to use a more elaborate methodology for determining material behaviour, as explained in this paper. For example, a typical circular test coupon 10 mm in grip diameter narrowing to a gauge diameter of 5 mm is reasonable if the rail head has uniform hardness; but with the surface hardened rails, there is a good chance of missing the actual material properties at the rail surface, thus leading to inaccurate material model data being obtained.

Heat treated head-hardened rail steel exhibits a non-uniform distribution of material properties due to variations in manufacturing and heat treatment processes. Any non-uniformity could give rise to excessive sub-surface plastic strain accumulation from unintended material softness that could lead to damage and failure of the rail head. Moreover, the material layers removed by wear and preventive maintenance grinding potentially expose the softer regions of the rail head to the surface. Consequently, rail service life will be reduced substantially, especially at small-radius curves.

Such behaviour may also be exhibited in premium rails which have undergone additional thermal modification, such as where connections are made using, for example, the flashbutt welding technique. Mutton *et al.* [14] observed that softening of the rail in the heat affected zone (HAZ) can lead to increased gauge corner cracking and severe plastic deformation. Their research also studies the hardness deviation and microstructural changes in the HAZ area of the weld joint.

In this paper, the limitations and effects of the sampling depth on the ratcheting and fatigue response of head hardened rail steel are investigated. Moreover, microstructural characterization of the rail head is conducted to investigate the relationship between mechanical and metallurgical properties of the material.

2 Experimental Approach

2.1 Material

The material tested was cut from new 60 kg/m, grade AS1085.1 rail, with elemental composition given in Table 1. The material microstructure was studied at different depths in both transverse and longitudinal directions. To aid visualisation of the microstructure the polished surfaces were etched with 5% Nital. In summary, the transverse section shows that the microstructure changes from fine pearlite to a coarse pearlite with increasing depth. Grain distortion and inclusions (MnS) can be observed in the longitudinal section due to the rolling process. The laminar spacings of pearlite microstructures were recorded using Zeiss SEM images at different rail head depths as shown in Fig. 2.

2.2 Sample location

As the material properties vary down the cross-section of the rail head, it is important to select the sampling location with care. Sampling positions were chosen according to the hardness profile and practical limitations related to cutting the samples from the rail head. As shown in Fig. 2, the top sample is very close to the rail-head surface while the fourth sample is 33 mm below the rail surface. According to the hardness profile (Fig. 1), the 1-5 mm layer exhibits high Vickers hardness (410-430 HV), which then drops significantly as the depth increases.

Rectangular-shaped test coupons (according to ASTM E466 specification) were obtained from each sampling location. The dimensions of the test coupons are shown in Fig. 3. A major problem with the rectangular shape is that the test coupon can buckle when subjected to compression during cyclic-loading. The rectangular specimens were therefore designed and machined with a low slenderness-ratio in order to mitigate buckling effects.

The test coupons were machined with a gauge length of 21 mm and rectangular cross-section dimensions of 6 mm by 10 mm. Before testing, the gauge surfaces were ground and polished to a mirror-like finish, free from scratches visible to the naked eye. This process was conducted to prevent crack initiation and premature failure due to surface defects.

2.3 Fatigue tests

Force-controlled tests were performed using the MTS 810 with TestStar II® control system, in accordance with standard ASTM E466 [15]. All test coupons were subjected to the same uniaxial cyclic loading conditions by keeping the force amplitude and mean force constant to study the different ratcheting and fatigue behaviours.

The uniaxial cyclic force-controlled test method used a triangular waveform and the axial load was controlled by means of load-cell feedback. During each test, the axial load-rate was maintained at 8.5 kN/s – equivalent to a stress rate of 140 MPa/s. A mean stress (σ_m) of 83 MPa and stress amplitude (σ_a) of 694 MPa were used. Cyclic loading was carried out until stabilization of the ratcheting cycle or reaching the critical strain level (0.1).

The uniaxial strain-controlled tests used a triangular waveform for strain application with different mean amplitudes and slower strain rate in order to obtain optimum control. During the tests, strain amplitudes (ε_a) of 0.5%, 1.0% and 1.5% were used with mean strain values (ε_m) of 0%, 0.5% and 1.0% respectively. Identical strain controlled tests were conducted for each level with 0.0005 /s strain rate.

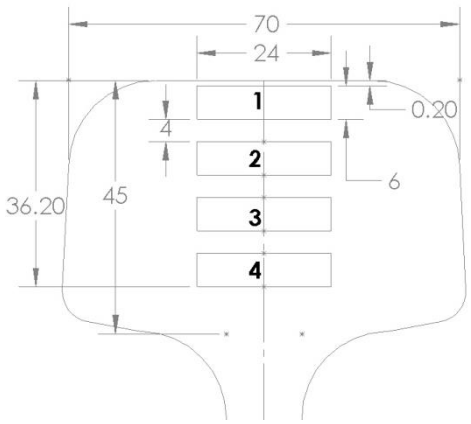

Fig. 2. Sampling positions in the rail head.

2.4 Hardness tests

Hardness was measured at different positions on the rail cross-section using a micro-Vickers hardness tester (Matsuzawa MXT70) in order to then calculate yield strength variation across the sample. Sample preparation and hardness measurements (HV100) were made according to standard ASTM E384 [16]. At each sample depth-level, two hardness measurements were also made in the longitudinal section to evaluate uniformity of material properties at the given location. Standard ASTM E122-72 [17] was followed to determine the sample size necessary to obtain the mean hardness with a 95% confidence level.

3 Results and Discussion

3.1 Microstructure of rail steel

The rail microstructures have been identified as ferrite and cementite layers of varying refinement. Due to induction hardening, different pearlites and upper bainitic microstructures exist. As shown in Fig. 4, the microstructure varies both in longitudinal and transverse directions. Near the rail surface (0.2 mm depth), pro-eutectoid cementite is observed within the prior-austenite grain boundaries (indicated by yellow arrows in Fig. 4 b) probably due to the high carbon content of the rail steel.

Garnham *et al.* [18] highlighted that the presence of pro-eutectoid cementite is undesirable as it is a source of embrittlement and reduces the wear and rolling contact fatigue resistance of the steel. The darker region in Fig. 4 a) represents fine pearlitic and upper bainitic structures. The bottom level test coupon showed a coarse pearlitic structure with the lamellae-spacing observable in Figs. 4 c) and d).

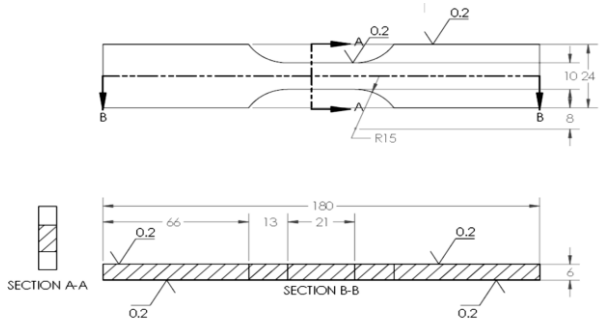

Fig. 3. Rectangular test coupon dimensions.

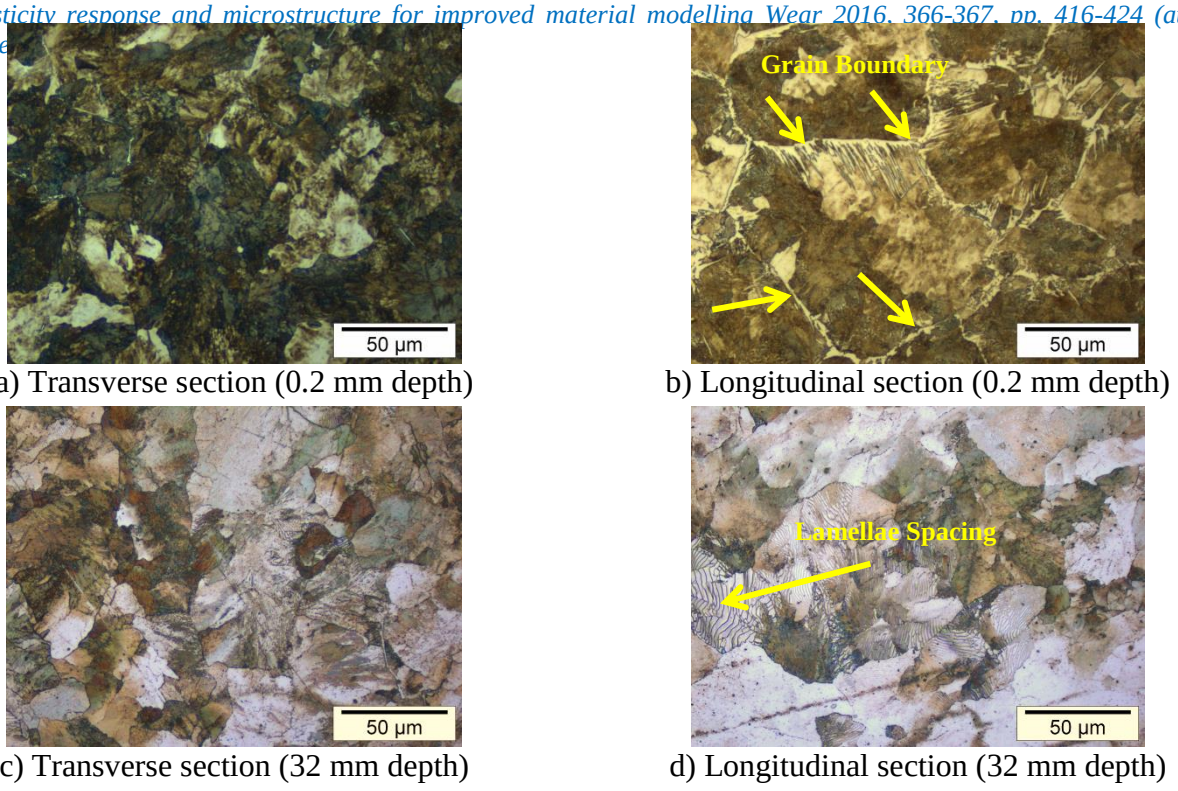

a) Transverse section (0.2 mm depth) b) Longitudinal section (0.2 mm depth)

c) Transverse section (32 mm depth) d) Longitudinal section (32 mm depth)

Fig. 4. Microstructure of the rail head for longitudinal and transverse cross-sections at two different depths.

Further investigations have been conducted on the transverse-direction microstructure of the test coupons. As shown in Fig. 5, the laminar spacing of the microstructure increases with respect to sampling position. Impurities (MnS by elemental analysis) may be observed in Fig. 5 d) interspersed within the microstructure and disturbing the formation of the pearlitic structure.

According to Sunwoo *et al.* [19], the cyclic deformation characteristics, i.e. the tendency for cyclic softening/hardening, of a material, is strongly dependent on its lamellar spacing. The proper quantification of the spacing between cementite layers was conducted using ImageJ software on the SEM images. The brightness profile of the image can be recorded along a line drawn perpendicular to the laminar layers (refer Fig. 6).

It is important to note that the images were taken at different tilting positions relative to the sectioned sample to obtain maximum laminar density. Then the profile contouring line was drawn perpendicular to the laminar layers in order to eliminate any angular effects of the lamellae. The cementite phase is represented by the peaks, while the ferrite phase is represented by the valleys, as shown in Fig. 6.

The distance between each consecutive peak and valley determines the inter-lamellar spacing. At each sampling level, more than 175 random inter-lamellar spacing's were considered and a statistical analysis of the distance was performed to obtain 95% confidence intervals for the mean of the sample.

The experimental results of mean inter-lamellar spacing are presented in Table 2. They demonstrate that inter-lamellar spacing increases along the depth of the rail head due to an inverse relationship between inter-lamellar spacing and undercooling conditions [20]. The rail head is exposed to large undercooling during the manufacturing process, so fine inter-lamellar spacing results near the rail surface.

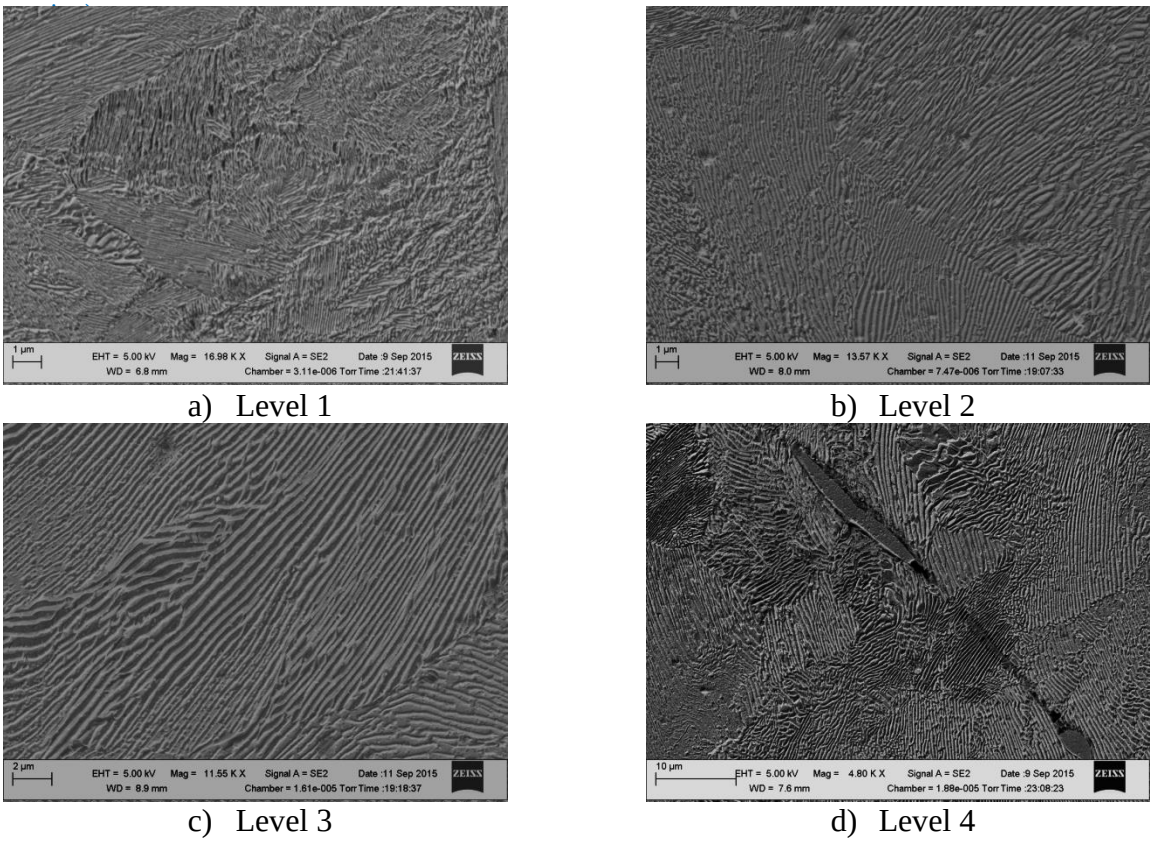

a) Level 1 b) Level 2

c) Level 3 d) Level 4

Fig. 5. Zeiss FESEM images of the each level test coupon.

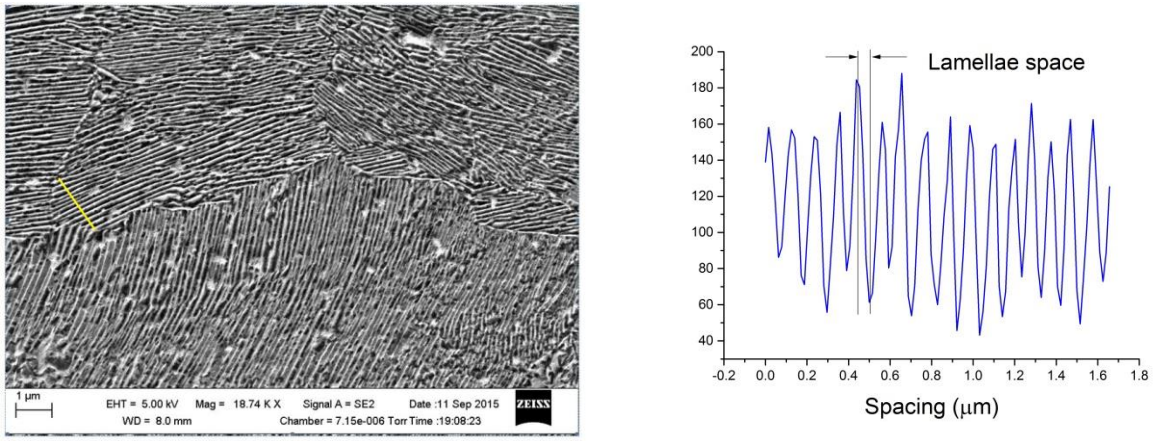

Fig. 6. Brightness profile along the drawn line.

3.2 Estimation of mean hardness of test coupon

The Standard ASTM E122-09 is followed to determine the sample size needed for each test coupon in order to obtain a statistically significant measure of mean hardness,

$$n = \left(\frac{3SD}{SE}\right)^2 \qquad \textbf{(1)}$$

where n is the estimated sample size, SD is the estimate of standard deviation and SE (the standard error) is the maximum acceptable difference between the true average and sample average. According to standards data, rail hardness can vary from 300-430 HV and, therefore, it was assumed that the hardness

Table 2. Microstructure and mechanical properties data summary.

Level / Depth (mm)	Laminar spacing, λ (nm)	Standard deviation of spacing (nm)	Yield strength at 0.2% strain (MPa)	Mean hardness (HV100)	H_v uncertainty (HV100)
Level 1 / 0.2	44	±12	911	415.6	±4.2
Level 2 / 10.2	63	±14	805	381.6	±8.3
Level 3 / 20.2	122	±36	572	302.2	±6.5
Level 4 / 30.2	189	±59	510	282.1	±7.9

is normally distributed with standard error, SE=12 HV. The calculated standard deviation is SD=21.97 MPa and the sample size needed to estimate the hardness of the test coupon is therefore n=30.

The recorded 30 random hardness values of the each test coupon are illustrated in Fig. 7. If the sample size is equal to 30 or more, then the following equations can be used to calculate the standard deviation (SD) and mean ($\overline{X}$), as the data has a z-distribution.

$$SD = \sqrt{\sum_1^n \frac{(X_i - \overline{X})^2}{n-1}} \qquad \textbf{(2)}$$

$$\overline{X} = \frac{\sum X_i}{n} \qquad \textbf{(3)}$$

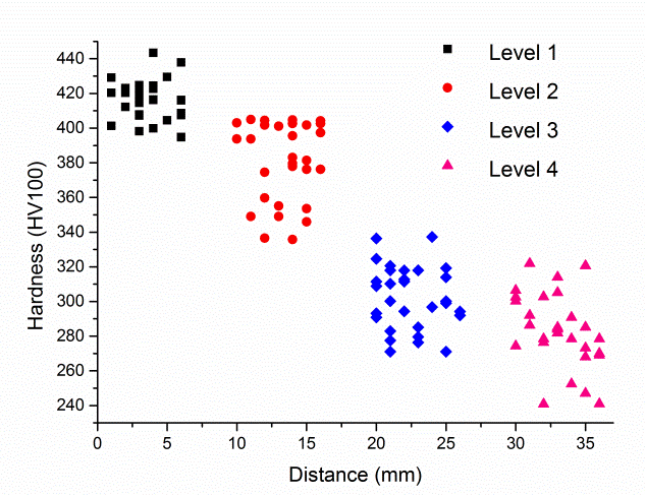

Fig. 7. Hardness profile of the test coupon.

Finally, the population mean (μ) is estimated using the following equation for 95% confidence interval for z-distribution when the sample size is equal to 30. The estimated mean hardness values are summarised in Table 2.

$$\boldsymbol{\mu = \overline{X} \pm z \times \frac{SD}{\sqrt{n}}} \qquad \textbf{(4)}$$

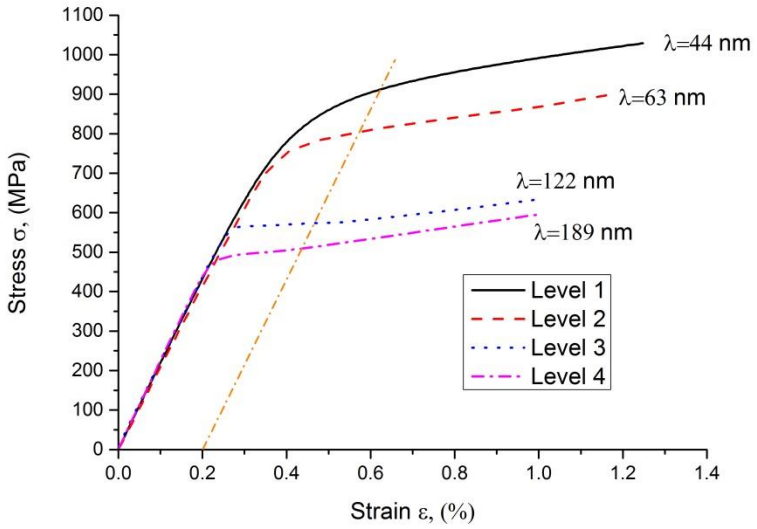

Fig. 8. Tensile stress and strain behaviour of specimens at different depths (refer Fig. 2) from the surface.

3.3 Stress-controlled test

The rectangular-shaped specimens obtained from the rail at different depth levels were tested under the same conditions of room temperature with predefined stress amplitude and mean. Close observation of the tensile stress-strain curves in Fig. 8 shows significant variation between samples of elongation in the first load cycle. For example, the level 4 sample exhibited about five-times greater elongation than the level 1 (top) sample under otherwise identical conditions. Also, yield stress diminishes with increasing depth; the bottom test coupon yield stress is 45% less relative to the top test coupon. Furthermore, precise material

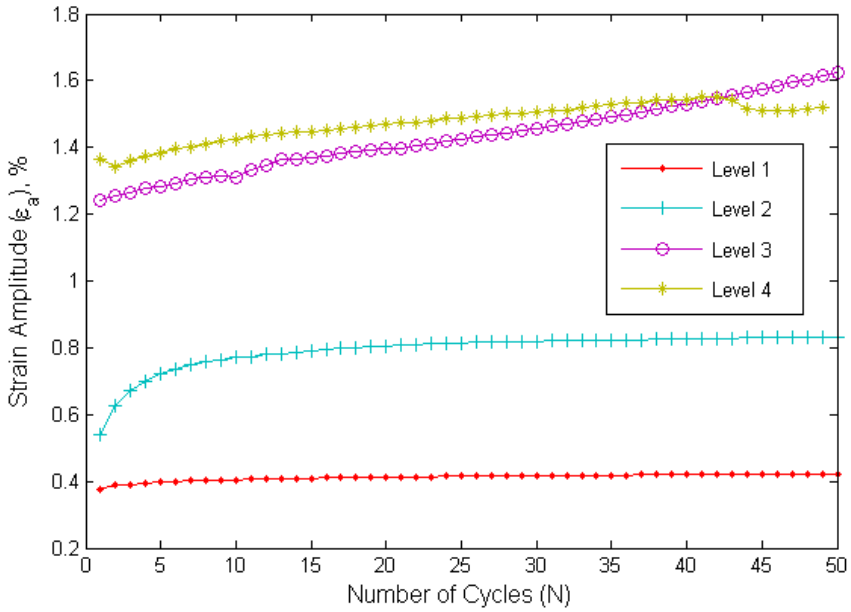

Fig. 9. Strain amplitude at different depths (refer Fig. 2) versus number of cycles.

properties are obtained, as the 0.2% yield point for the level 1 sample is 911 MPa; which is significantly greater than the yield of 780 MPa that would be obtained from a round test coupon.

The strain amplitude variation is plotted in Fig. 9 and it may be clearly observed that strain amplitude is higher at greater depth, under otherwise identical test conditions. The material becomes weaker with depth and exhibits greater tendency to deform plastically. The first two specimens exhibit a plateau in the strain amplitude as the material properties stabilize with further loading cycles.

The strain amplitudes of level 1 and 2 test coupons plateau after about the 5^{th} and 10^{th} cycles respectively due to cyclic hardening and stabilisation of the ratcheting phenomenon. There appears to be no stabilisation with the other two test coupons as the strain amplitude continues to grow (softening effect)

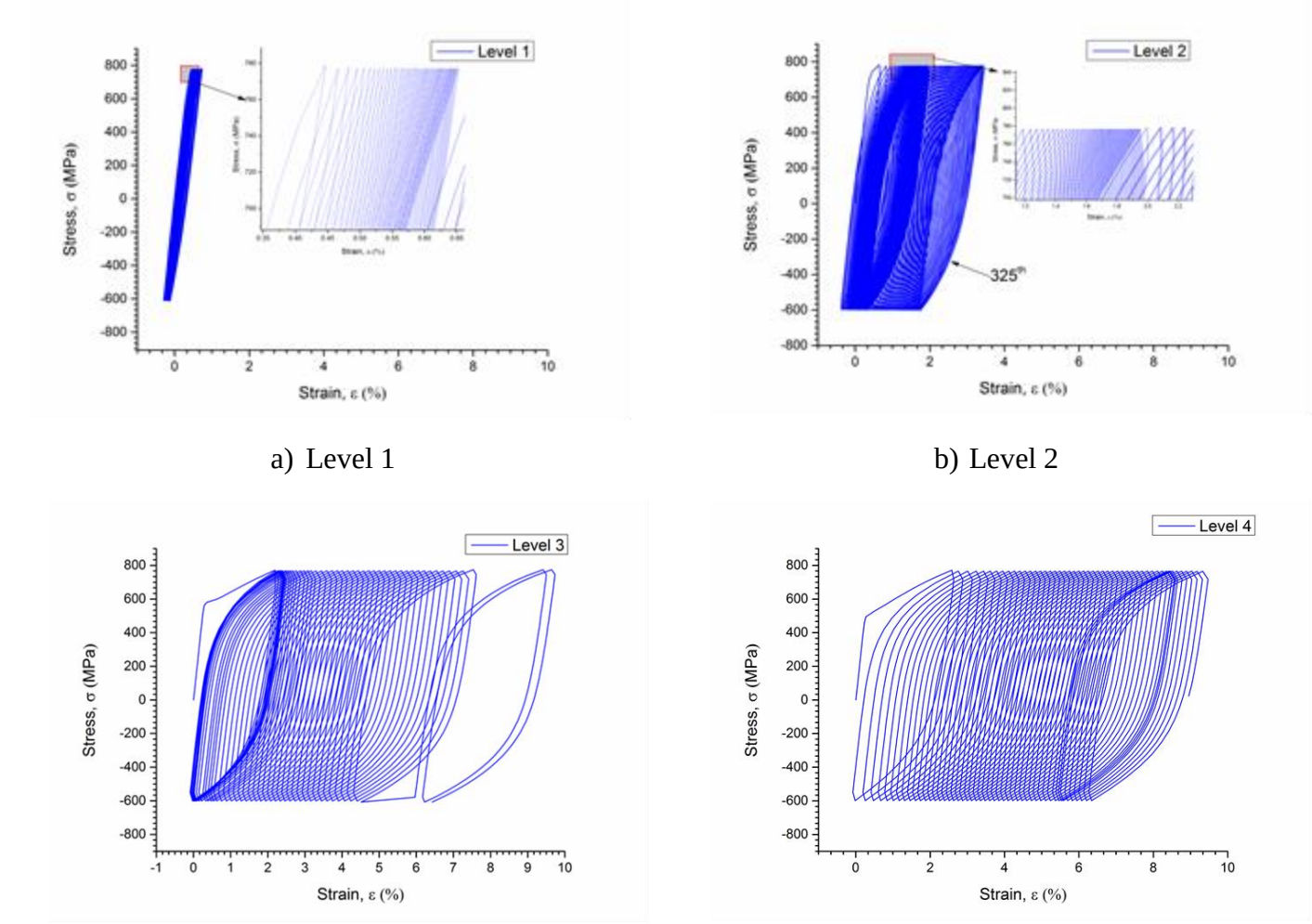

a) Level 1

b) Level 2

c) Level 3

d) Level 4

Fig. 10. Stress-controlled stress-strain curves for the different sampling depths (refer Fig. 2).

with increasing number of cycles. Furthermore, the level 1 test coupon shows a small hysteresis loop area compared to the level 4 coupon; the latter absorbing far greater strain energy due to the increased nucleation and mobility of dislocations. Each test exhibited a smaller hysteresis curve area in the beginning which gradually expands as the number of cycles progresses. This may be explained by the fact that plastic deformation in the test coupon initially occurs locally and then gradually expands throughout the gauge volume. The experimental cyclic stress-strain data is shown in Fig. 10 and illustrates the very different

softening and hardening behaviours of the rail steel at different depths under the same force-controlled conditions.

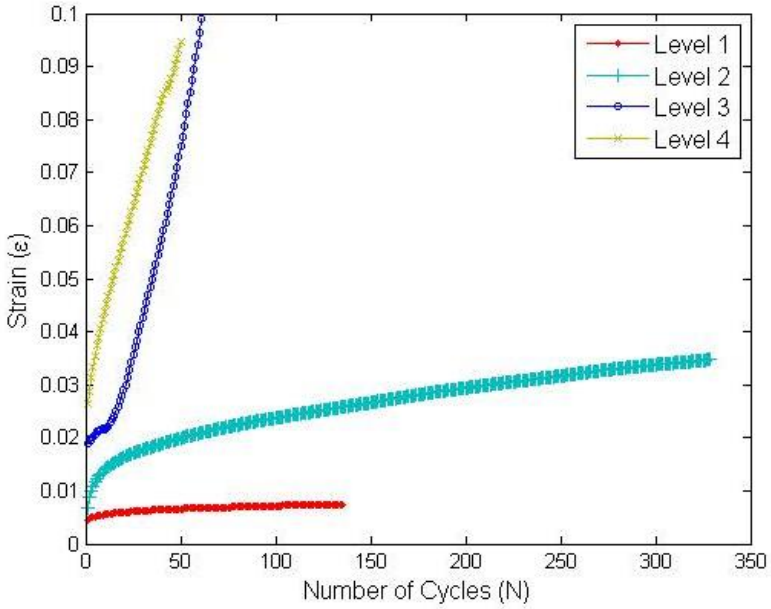

Fig. 11. Ratcheting strain curves for each test coupon.

It may be observed that the first and second test coupons exhibited cyclic hardening behaviour as the hysteresis loops contracted with increasing number of cycles, while the level 3 coupon exhibited expanding loops typical of softening behaviour. The level 4 coupon showed cyclic hardening behaviour up to the 42nd cycle, then the hysteresis loops expanded with increasing number of cycles suggesting softening behaviour. This unusual behaviour is possibly a result of the production process (hot rolling) as Level 4 is close to the lower rail head surface or some other cause that has yet to be identified.

The plastic strain behaviour of the four different samples is shown in Fig. 11. It may be observed that the ratcheting strain-rate reduced with loading cycles, and the upper two test specimens showed very low, stable ratcheting rate as the strain amplitude stabilised in the later loading cycles; the lower two specimens, however, showed higher ratcheting rate.

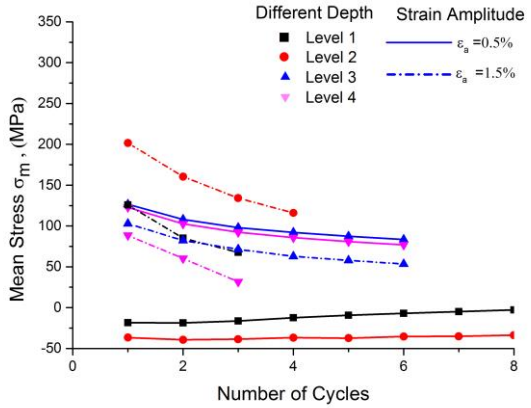

Fig. 12. Mean stress of hysteresis at different depth levels.

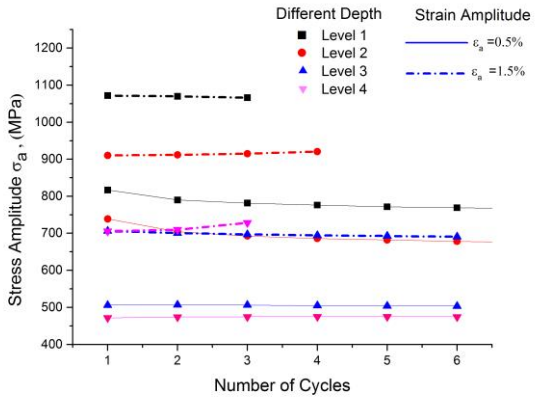

Fig. 13. Stress amplitudes of hysteresis at different depth levels.

The microstructure of the rail steel varied with the depth. In the top layer it has a mix of bainitic and pearlitic structures (Fig. 5 a) while the bottom layer has a coarse pearlitic structure (Fig. 5 e). A tendency towards hardening is observed near the top and softening behaviour is observed in the lower test coupons. This is consistent with Sunwoo's research [19]; i.e. steel with coarse pearlite structure is softer when compared to bainite and fine pearlite structures.

Ratcheting curves for each depth level are shown in Fig. 11. Higher ratcheting strain is observed corresponding to increased depth under the same force controlled test conditions. The bottom two test coupons exhibit high ratcheting rates leading to failure after relatively few loading cycles.

3.4 Strain-controlled test

The resultant mean stress and stress amplitude developed in the strain controlled hysteresis loops are shown in Figs. 12 and 13 respectively. As expected, in the lower strain amplitudes (0.5%), there is a trend towards a zero mean stress level. However, the upper level shows higher compressive stress due to higher hardness and also greater resistance to buckling at higher strain amplitudes (up to 1%). The bottom two specimens, on the other hand, start buckling at 0.75% strain amplitude. In order to control such effect a positive mean strain was introduced to the different strain amplitudes.

According to Fig. 13, the stress amplitudes maintain reasonably steady levels during the cyclic loadings. The stress amplitudes naturally rise as the strain amplitude is increased. Moreover, the stress amplitude decreases with increasing depth for a given strain amplitude, with material softening behaviour evident beyond a certain depth level. As shown in Fig. 13, the stress required to accumulate plastic strain is on average 25-45% less than that at the rail's top surface. Furthermore, it is highlighted that material behaviour changes significantly between level 2 and level 3 (10 to 20 mm).

3.5 Hysteresis loops

The hysteresis loops for the strain controlled tests are shown in Fig. 14. The loops have been translated to the zero mean stress and strain levels for better presentation and simulation purposes. The hysteresis loop's strain energy increased with the strain amplitude as expected. But strain energy decreases with depth from the rail head as the material reduces in hardness.

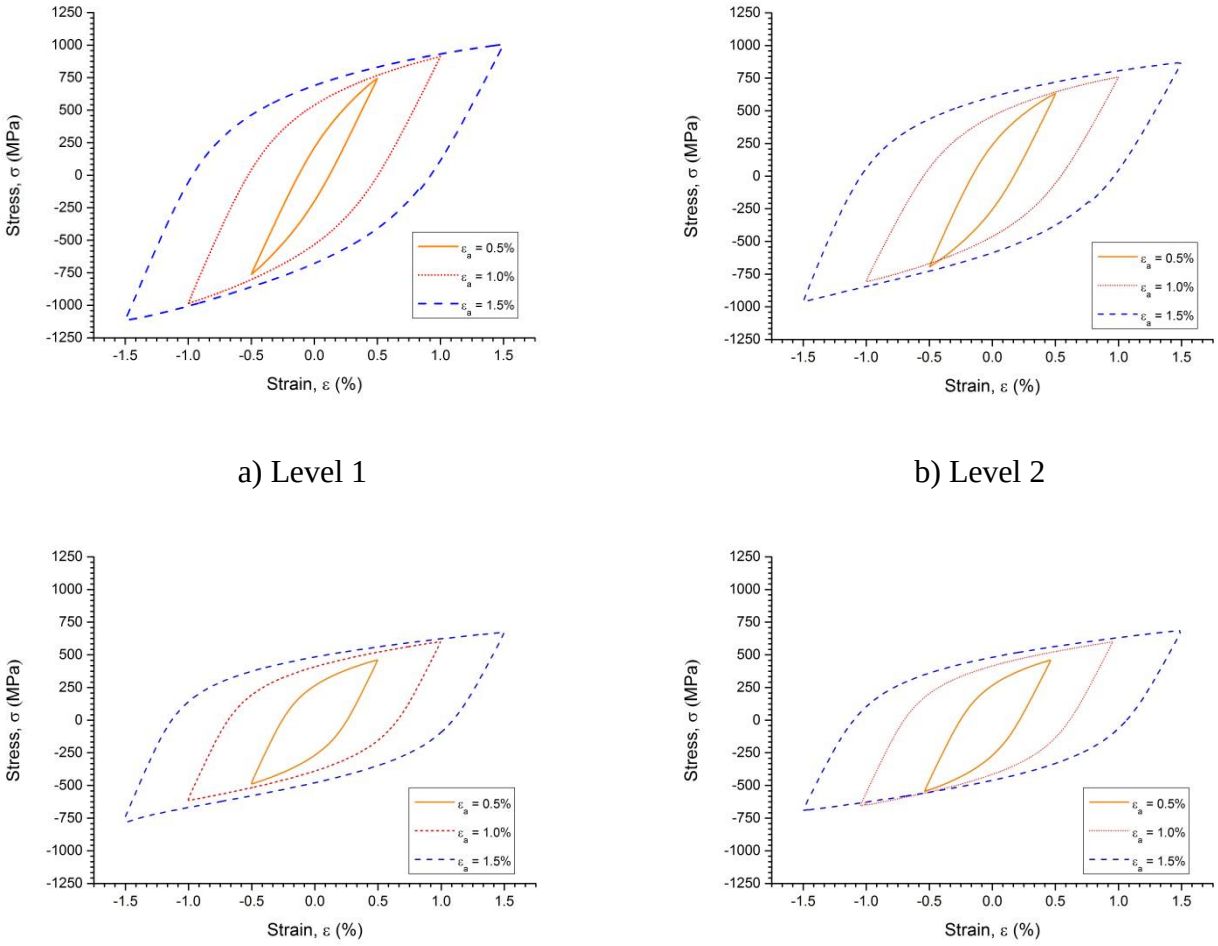

a) Level 1 b) Level 2

c) Level 3 d) Level 4

Fig. 14. Stabilised hysteresis loops at different depth levels.

Comparison of the hysteresis loops at 1.5% strain amplitude at different depth levels is illustrated in Fig. 15, demonstrating clearly the softening behaviour with increasing depth and the diminishing hardening effect towards that exhibited by plain carbon steel.

The rectangular-shaped specimens are capable to capture material properties gradient of the heat treated rail steel. Of course there are some limitations with the buckling effect; however, careful experiment execution is able to rectify such limitations.

3.6 Comparison mechanical and metellurgical parameters

The inter-lamellar spacing and hardness of the test coupons shows clear correlation, as shown in Fig. 16. Finer inter-lamellar spacing makes a hard cementite arrangement that corresponds to increased hardness of the rail material. Moreover, it is noticed that strain amplitude (ε_a) increases together with inter-lamellar spacing while yield strength drops drastically due to the higher inter-lamellar spacing which has more ferrite. Ferrite is well known for its softness and crack initiation behaviour [19]. Moreover, the fine inter-lamellar spacing shown in the top level sample is similar to the premium rail used in Australia [21],

but the non-uniform cooling process results in more than four-times higher spacing in the bottom test coupon.

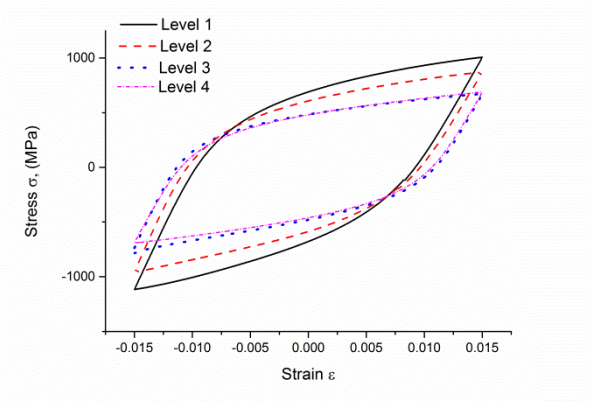

Fig. 15. Material response at 1.5% strain amplitude at different depth levels

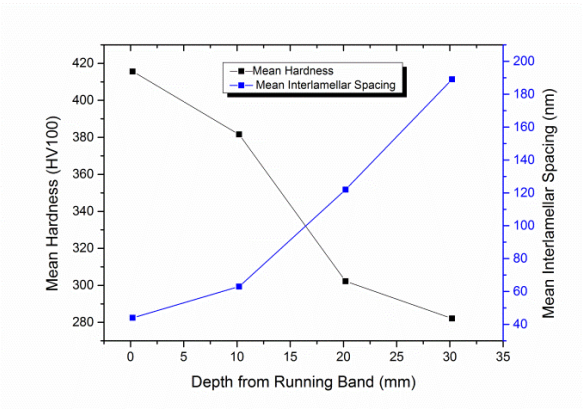

Fig. 16. Hardness and interlamellar spacing

The data presents an important trait of head hardened rail steel: after a certain depth from the rail surface (between second and third coupons in this instance) there is a transition in material ratcheting behaviour attributed to microstructural differences arising from the hardening process.

Ratcheting is an important mechanism in rail wear, crack initiation and growth. The cyclic load test-results clearly show how material at different depth from the rail surface can behave very differently under cyclic loads which have the potential to induce significant plastic deformations.

Samples obtained from the rail sections by Tyfour *et al*. [7, 8] exhibited a high likelihood of material property inhomogeneity. When the sample wheels were subjected to rolling contact tests in the rail test rig, part of the wheel could likely have an increased tendency to reach rolling-contact fatigue failure prematurely due to high ratcheting rates. Under such circumstances the data obtained would possess low accuracy when attempting to model and predict rail surface damage and wear.

The rectangular-shaped specimens showed capabilities to capture material properties with higher resolution when compared to cylindrical test coupons. However there are some limitations that exist with rectangular-shaped specimens. They are more susceptible to buckling during strain controlled tests with higher strain amplitudes and they cannot easily be used in biaxial tests which are important in advanced material model calibration. It is also important to highlight that it is difficult to characterise gauge corner material properties with the suggested test coupon dimensions; however, modified test coupons could be used in further studies.

These observations provide motivation to improve rail material modelling by considering the variations that occur depending on the location from which the samples are taken, ultimately leading to increased reliability of simulation and modelling results.

4 Conclusion

From the cyclic tests conducted, together with microstructural characterisation and hardness testing of AS1085.1 rail steel, the following conclusions can be drawn:

1. The experimental approach presented in this work is very useful for obtaining detailed cyclic loading and ratcheting material data necessary for effective material behaviour modelling.
2. Rectangular-shaped test coupons provide more accurate sampling of material properties compared to cylindrical ones in rail heads where significant material inhomogeneity exists. The more accurate data and material models that can be obtained will lead to improved rail surface wear simulation and prediction.
3. Inter-lamellar spacing strongly correlates with the cyclic softening and hardening of the head hardened rail steel. This data can be used to extrapolate material cyclic properties for head hardened rail steels based on hardness measurements.
4. This study also highlights that rail discs obtained from the rail head for twin disc tests are more prone to develop surface defects when compared to real service conditions, especially if significant material property gradients exist in the rail head.
5. The more precise sampling method presented lends itself to better analysis of rolling contact fatigue behaviour due to localised material inhomogeneity arising from, for example, rail welding techniques.
6. This work raises attention to the limitations of existing practices in material sampling and suggests an improved approach.

Acknowledgments

This investigation has been performed within the Materials Laboratory in the Queensland University of Technology. The authors would like to thank Anthony Morris, Gregory Paterson and Sanjleena Singh for their assistance and guidance with this research.

References

[1].J. Kirk, *Fortescue opens the world's heaviest haul railway.* Railway Gazette International., July 2008: p. 427.

[2].C.L. Pun, Q. Kan, P.J. Mutton, G. Kang, and W. Yan, *Ratcheting behaviour of high strength rail steels under bi-axial compression–torsion loadings: Experiment and simulation.* International Journal of Fatigue, 2014. **66**: p. 138-154.

[3].D.D. Hagarty, *A Short History of Railway Track in Australia - 1 New South Wales.* Australian Railway Historical Society Bulletin, February 1999: p. 55–67.

[4].A. Kapoor, J.H. Beynon, D.I. Fletcher, and M. Loo-Morrey. *Computer simulation of strain accumulation and hardening for pearlitic rail steel undergoing repeated contact*. 2004. Professional Engineering Publishing Ltd.

[5].A. Kapoor, D.I. Fletcher, F.J. Franklin, G. Vasic, and L. Smith. *Rail-wheel contact research at the University of Newcastle*. in *11th International Conference on Fracture 2005, ICF11, March 20, 2005 - March 25, 2005*. 2005. Turin, Italy: International Congress on Fracture.

[6].J.W. Ringsberg, *Life prediction of rolling contact fatigue crack initiation.* International Journal of Fatigue, 2001. **23**(7): p. 575-586.

[7].W. Tyfour, J. Beynon, and A. Kapoor, *The steady state wear behaviour of pearlitic rail steel under dry rolling-sliding contact conditions.* Wear, 1995. **180**(1): p. 79-89.
[8].W. Tyfour, J. Beynon, and A. Kapoor, *Deterioration of rolling contact fatigue life of pearlitic rail steel due to dry-wet rolling-sliding line contact.* Wear, 1996. **197**(1): p. 255-265.
[9].A. Kapoor, F.J. Franklin, S.K. Wong, and M. Ishida, *Surface roughness and plastic flow in rail wheel contact.* Wear, 2002. **253**(1-2): p. 257-264.
[10].J. Seo, S. Kwon, H. Jun, and D. Lee. *Rolling contact fatigue of white etching layer on pearlite steel rail*. 2010. Laubisrutistr.24, Stafa-Zuerich, CH-8712, Switzerland: Trans Tech Publications Ltd.
[11].J. Ahlström and B. Karlsson, *Fatigue behaviour of rail steel—A comparison between strain and stress controlled loading.* Wear, 2005. **258**(7-8): p. 1187-1193.
[12].G.Z. Kang, Q. Gao, X.J. Yang, and Y.F. Sun, *Strain cyclic characteristics and ratcheting of U71Mn rail steel under uniaxial loading.* Acta Metallurgica Sinica (English Letters), 2000. **13**(3): p. 893-900.
[13].X. Yang, *Low cycle fatigue and cyclic stress ratcheting failure behavior of carbon steel 45 under uniaxial cyclic loading.* International journal of fatigue, 2005. **27**(9): p. 1124-1132.
[14].J.C. Peter Mutton, Cong Qiu and Darrien Welsby, *Microstructural Characterisation of Rolling contact Fatigue Damage in Flashbutt Welds*, in *10th International Conference on Contact Mechanics CM2015*2015 September: Colorado Springs, Colorado, USA.
[15].A. Standard, *E466.* Standard practice for conducting force controlled constant amplitude axial fatigue tests of metallic materials. West Conshohocken, PA: ASTM International, 2007.
[16].A. Standard, *E384, Standard Test Method for Knoop and Vickers Hardness of Materials.* ASTM International, 2011.
[17].A. Standard, *E122-72 Standard recommended practice for choice of sample size to estimate the average quality of a lot or process.* ASTM Philadelphia, PA.
[18].J.E. Garnham and C.L. Davis, *The role of deformed rail microstructure on rolling contact fatigue initiation.* Wear, 2008. **265**(9): p. 1363-1372.
[19].H. Sunwoo, M. Fine, M. Meshii, and D. Stone, *Cyclic deformation of pearlitic eutectoid rail steel.* Metallurgical Transactions A, 1982. **13**(11): p. 2035-2047.
[20].N. Ridley, *A Review of the Data on the Interlamellar Spacing of Pearlite.* Metallurgical Transactions A, 1984. **15**(6): p. 1019-1036.
[21].Chung Lun Pun, Kim Chuan Sho, Peter Mutton, and W. Yan, *Microstructural Characterization of High Strength Rail Steels*, in *10th International Conference on Contact Mechanics CM2015*2015 September: Colorado Springs, Colorado, USA.